

A high efficiency tile-fiber hodoscope read out by multichannel phototubes

P. Cushman*, S. Giron, J. Kindem, D. Maxam, D. Miller, C. Timmermans

University of Minnesota, Minneapolis, MN, USA

Received 11 April 1996

Abstract

Plastic scintillator tiles of 7 mm × 8 mm cross section with an embedded green wavelength shifting fiber form the elements of an x - y hodoscope to be used in the g -2 experiment at Brookhaven. The fibers are read out through 1.5 m clear fibers by a new "low crosstalk" design of the Philips multi-channel photomultiplier tube XP1723/D1. An average light yield of 30 photoelectrons are produced in a standard bialkali tube per minimum ionizing particle. Detection efficiencies of 98.6% averaged across an assembled plane can be completely accounted for by the measured 110 μ m of paint thickness between elements. Data is presented on the light yield and attenuation of the hodoscope elements; the crosstalk, uniformity, and fast gating of the multichannel tubes; and the overall performance of the device in a test beam.

1. Introduction

An experiment to measure the anomalous magnetic moment of the muon to 0.35 ppm will begin taking data in Spring 1996 [1]. The centerpiece of this new experiment is a 14 m diameter superferric storage ring with a 1.5 T magnetic field homogeneous to 1 ppm. The spins of the stored muons, which are initially aligned with the momentum vector, precess in the magnetic field. The difference between the spin precession frequency and the cyclotron frequency, ω_a , is measured by counting the number of decay electrons above 1.6 GeV which strike 24 calorimeters, placed at equal intervals around the inner circumference of the storage ring, as a function of time. The number of forward-going, high-energy decay electrons striking a calorimeter has the functional form:

$$N(t) = N_0 e^{-t/\tau} [1 - A \cos(\omega_a t + \phi)], \quad (1)$$

where τ is the muon lifetime and ω_a is the g -2 precession frequency.

Since the calorimeters do not provide position information, a position sensitive detector (PSD) will be installed on the front face of the calorimeter. The purpose of such a detector is to reject events where two or more decay electrons strike the calorimeter within the same 5 ns time bucket. Two low energy electrons, which would otherwise be below threshold, could resemble one higher energy electron. These pileup events introduce a systematic bias in the fre-

quency measurement between early and late times since the event rate is exponentially decaying with the muon lifetime. In addition, vertical position information provides a limit on the electric dipole moment (edm) of the muon. The presence of an edm would tilt the plane of the spin precession, introducing an up-down wobble to the electron distribution. By being sensitive to a change of several millimeters in the mean of the vertical distribution, one can rule out an edm to 10^{-20} e cm.

The design requirements which have to be met for a PSD in the g -2 experiment are listed below:

- 1) Excellent efficiency for detecting minimum ionizing particles (MIPs).
- 2) Sufficient spatial segmentation to reduce pileup by a factor of 100.
- 3) Sufficient spatial segmentation in the vertical plane to be sensitive to an edm of $> 10^{-20}$ e cm.
- 4) Insensitivity to the initial burst (or "flash") of charged particles and neutrons caused by a fraction of the injected pions striking the storage ring walls without decaying to muons. During the 1-2 μ s of intense light produced by the flash, the phototubes connected to the PSD must be gated off to avoid saturation effects. In addition, tests using fast extracted beam at Brookhaven demonstrated the existence of a long-lived ($\tau \sim 30 \mu$ s) component to the flash which can introduce a bias in the g -2 frequency measurement from early to late times. A portion of this slow component can be eliminated by reducing the amount of plastic near the beam and preventing charged particles produced in the mid-plane of the ring from passing through the phototubes (i.e., the

* Corresponding author. Tel. +1 612 6247375, fax +1 612 6244578.



Fig. 1. An individual PSD tile.

phototubes must be located above or below the storage ring magnet, necessitating a long light guide). Another component, due to residual charge in the phototubes, can be reduced by improving the gating design of the tube, as discussed in this paper. A third component, background due to neutrons and photons produced inside the calorimeter and the surrounding C-shaped magnet, must be eliminated by loading the calorimeter with neutron absorbing material such as boron or lithium.

There are 24 calorimeters spaced around the inner circumference of the storage ring. The design of the PSD is a careful optimization of the competing requirements of good light yield, space limitations, and cost per channel. Since each PSD provides 52 channels of horizontal and vertical information, the cost is mainly in the readout. In order to keep the cost down, multichannel phototubes (MCPMTs) rather than individual phototubes are chosen for the readout. In order to match the small MCPMT pixel size, fiber readout is required. 1 mm diameter fibers are chosen because they are the largest diameter fibers which are still flexible enough to bend 90° in the 1.5 cm of space between the top of the detector and the surrounding magnet pole tips. In order to maximize the response to minimum ionizing particles, the tiles are made as thick as possible along the beam direction without sacrificing light yield in the central wavelength shifting fiber due to nonuniform light collection. In order to keep the transmission high, but the overall volume of plastic light guide low, clear fiber light guides run from the green wavelength shifting fibers to the MCPMT, which is located out of the mid-plane, a meter away from the active area.

2. Detector design

Each PSD is a hodoscope consisting of one vertical and one horizontal plane which together cover a rectangular active area of 22.5 cm wide by 13 cm high. The segmentation is 7 mm, with 20 horizontal elements and 32 vertical elements. Each element is a 7 mm \times 8 mm cross-sectional strip of plastic scintillator, either 22.5 cm (horizontal) or 13 cm (vertical) long. The blue scintillator BCF404¹ was diamond-milled to an optical finish by Bicon and delivered in 4 mm \times 6.9 mm half-tiles, such that a 7 mm pitch could be achieved after painting. A semicircular groove was milled down the central axis of each half-tile using a ball-end mill. Multi-clad green wavelength shifting fiber (Kuraray Y11 (300ppm)-WLS)² of 1.0 mm diameter was glued into place in the groove and the other half-tile glued on top. The epoxy (EPO-TEK 310)³ was specially chosen because of its reasonable match to the index of refraction of the plastic and its low shrinkage upon curing, thus minimizing the formation of voids around the tile-fiber interface. After gluing and cleaning, the far end of the tiles was coated with 8000 Å of aluminum via an electron beam evaporation process. The other surfaces of each tile were painted with white reflective paint (NE 560)⁴ to prevent crosstalk between tiles. In an earlier prototype of the PSD, the tiles were wrapped in two layers of 0.1 mm medium density Teflon tape. Later testing showed that reflective paint only slightly (< 5%) diminished total light output of the tiles, was much easier

¹ Bicon Corp., 12345 Kinsman Rd., Newbury, OH 44065, USA.

² Kuraray International Corp., 200 Park Ave., New York, NY 10166, USA.

³ Epoxy Technology Inc., 14 Fortune Dr., Billerica, MA 01821, USA.

⁴ Nuclear Enterprises Technology, Inc., 9 Deer Park Dr., Monmouth Junction, NJ 08852, USA.

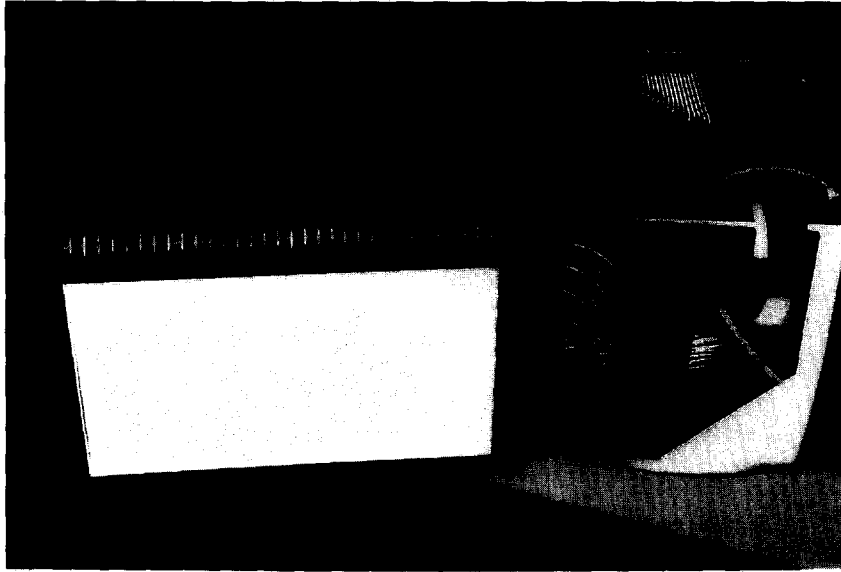


Fig. 2. The PSD mounted on the calorimeter.

to apply, and resulted in a smaller gap between elements. A picture of individual tiles in several stages of completion is shown in Fig. 1.

A stub of green fiber protrudes from the non-aluminized end of the tile. To assemble the PSD, the fiber stub of each tile is glued into counter-sunk holes in a bar of black Delrin⁵, 4.3 mm thick. The 1.05 mm diameter holes have a 7.0 mm center-to-center spacing. The fiber/Delrin/epoxy surface is flycut to provide an optically flat surface. A second Delrin bar with identical hole spacing is machined to hold a set of clear fibers of the same diameter. Although improved light transmission can be obtained by mating larger diameter clear fibers to the wavelength shifter, the thicker fibers would require a larger bending radius. Alignment pins and set screws in the Delrin bars are interspersed between each fiber hole to press the two bars together, yet allow for easy assembly and interchangeable pixel arrangements. The other end of the clear fiber bundle is potted into a Delrin cookie which matches the pixel arrangement of the MCPMT. Transmission loss through the interconnect was measured to be approximately 25%. The use of optical grease had negligible effect when the bars were tightly compressed. A photograph of the assembled PSD mounted on the front of the calorimeter station is shown in Fig. 2.

3. Tile characteristics

A scintillator with embedded wavelength shifter is a means of concentrating the light produced along the ionizing particle's path into a smaller readout area, thus enabling

one to mate 1 mm light guides to 7 mm × 8 mm scintillator tiles without losing a factor of 50 in light output due to simple area reduction. The light emitted into 4π from the blue fluor has numerous chances to intersect the central fiber and be reemitted in the green. Green light emitted within the fiber's critical angle will be piped to the end. Since the tiles are relatively short, attenuation is small (see Section 7.1) and even the light which goes in the opposite direction is collected after reflection from the aluminized end. Aluminization improves light collection efficiency by a factor of 30%. Originally it was believed that total internal

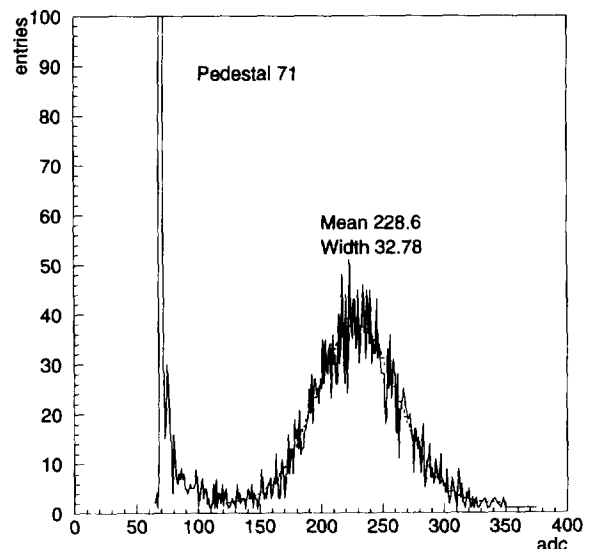


Fig. 3. ADC pulse height distribution of sample tile exposed to triggered betas from a ^{106}Ru source.

⁵ DuPont Engineering Plastics, 1007 N. Market St., Wilmington, DE 19898, USA.

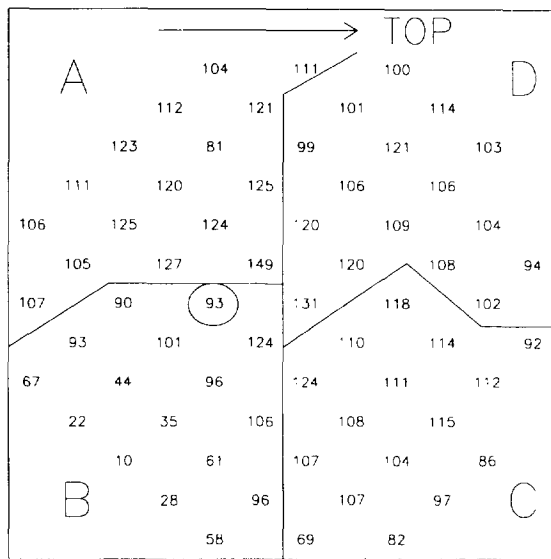


Fig. 4. Gain map for the MCPMT used in the beam test.

reflection from the tile surface was necessary to maintain a high light yield. This led us to diamond mill our tiles and wrap them in a white diffuse reflecting tape such as teflon or Tyvek⁶. When it was discovered that white paint (having no air gap interface) did almost as well as wrapping, we also tested painted tiles milled with a standard fly-cut fine-machined finish, and found no difference. This drastically reduces the labor, and thus the cost of each tile, since they can be machined in our local shop.

Before assembling the detector, tests were performed on sample tiles using a Ruthenium source (4 mCi ¹⁰⁶Ru) embedded in a small beamline composed of a permanent magnet tuned to direct the electrons (3.541 MeV end point energy) down a 5 mm diameter curved channel. This reduced contamination from gamma rays and lower energy betas. A trigger fiber behind the tile ensured that only electrons which made it through both scintillators were included in the sample.

The response of the tiles to minimum ionizing particles was established using a high resolution, photon counting tube (Hamamatsu R1332). The R1332 has a bi-alkali photocathode with a nominal quantum efficiency of 25% in the blue and 12% in the green and was calibrated in the lab by measuring the response to one and two photoelectrons. A plot of the ADC pulse height distribution from a typical tile exposed to the source is shown in Fig. 3, where the signal mean corresponds to 38 photoelectrons. Poisson statistics applied to the width of the curve gives a somewhat lower number of 23 p.e.

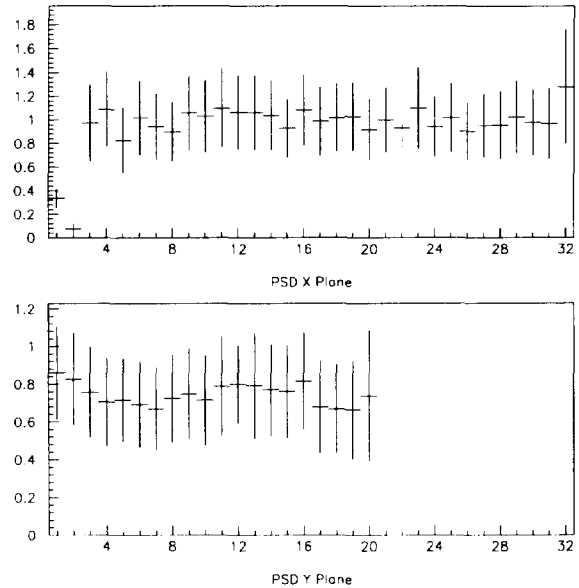


Fig. 5. PSD tile uniformity (Prototype II) with MCPMT channel-to-channel variations divided out. The two low channels in the x-plane are due to a bad hybrid in the ADC.

4. MCPMT characteristics

The Philips XP1700 series are multichannel photomultiplier tubes (MCPMT) with 64 or 96 independent amplification channels. They have 10 amplification stages and a nominal gain of 10^6 (see Comby and Meunier [2] for tube design details). They can be run with negative output signals (output operating as anode) or in a higher gain mode with the segmented output functioning as a dynode, producing positive signals. Linearity is good in both modes, with an appropriate choice of base resistances. We chose to run in positive mode in order to take advantage of the increased gain, thus eliminating the need for preamplifiers. The photocathode is typically run at negative 1000–1400 V with the anode at positive 25–75 V. The 64 output pins and 9 dynode inputs make contact with a printed circuit board via spring-loaded pogo pins. The circuit board is a resistive base plus signal fan-out, taking an 8×8 array with 0.1 in. pin spacing to four 17-pair ribbon cable connectors. The double-sided fan-out board is carefully designed to minimize electrical crosstalk ($< 1\%$). The anode grid collects the charge from all channels to provide a negative summed signal which can be capacitively coupled to an output pin on one of the 17-pair connectors.

The tubes are equipped with a fiber optic window in order to reduce crosstalk between channels. In order to further reduce crosstalk, Philips developed a new tube design, where the 64 multiplication channels are spread out over the available tube area in a checkerboard pattern (XP1723/D1), which effectively removes all “nearest neighbors”. The DC crosstalk is $< 2\%$, as measured by a picoammeter in a position scan across the tube face with a constant source

⁶ DuPont Engineering Plastics, 1007 N. Market St., Wilmington, DE 19898, USA.

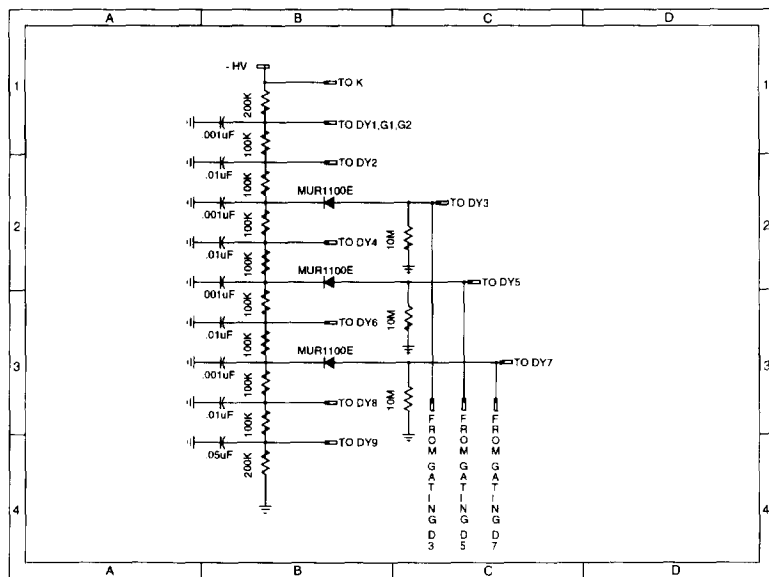


Fig. 6. Resistive base with gating circuit.

diode laser focussed to a 500 micron spot. However, there is a poorly understood inductive component which comes into play in the pulsed mode, and we have been unable to achieve better than 5-10% crosstalk for scintillator pulses. In order to confirm this effect, we performed studies with a light emitting diode pulse, varying its width between 50 ns to 1 ms. This clearly showed that the crosstalk improved in moving from AC to DC mode. Since we have a clear pulse above background, any crosstalk appears as a shoulder on the pedestal (see Section 7.3), and the threshold can be set to reject these events with minimal effect on the PSD efficiency. Details of the crosstalk, uniformity and rate dependence of these tubes has been studied by this group [3] and others [4] previously and is therefore not included here.

5. Uniformity of PSD response

The response of each of the MCPMTs were measured in the lab to determine the variation in gain response channel-to-channel. A nitrogen laser activated a small piece of blue scintillator. A coil of clear plastic fiber whose end was embedded in the scintillator, transmitted the light to the tube after an optical delay of 50 ns to avoid electrical noise induced by the laser switching circuits. The electrical noise was further reduced by enclosing the laser in an RF-shielded box. The fiber end was positioned far enough away from the tube such that the tube face was uniformly illuminated, which was verified by repeating measurements after various rotations and translations of the tube. Fig. 4 shows a gain map for the tube used in the beam test, where the numbers represent response normalized to the average over the complete set of pixels. Each sector, labelled A-D, was read out by one 17-pair twist-and-flat cable. The standard deviation

(σ_{N-1}/μ) was 26.9% and 59 pixels were within 50% of the tube average. Across our sample of five tubes, the average variation in gain between pixels was $\sigma_{N-1}/\mu = 26.1\%$ with an average of 60 pixels being within 50% of the tube averages.

A single PSD tile activated by the Ruthenium source was viewed by a standard channel of the MCPMT (circled on figure) as well as by the calibrated Hamamatsu R1332. Once the relative quantum efficiencies of the two tubes were accounted for, this provided a measure of the overall gain of the MCPMT. For the tube used in the test beam, the manufacturer measured a radiant intensity of 43 mA/W at 510 nm, corresponding to a quantum efficiency of 10.5% in the green. The overall tube gain, as defined above, was therefore 3×10^6 at an operating voltage of 1300 V and +20 V on the anode. The quantum efficiencies of the other tubes were generally lower, averaging 7% in the green. Note that this is an effective quantum efficiency which includes transmission loss through the fiber optic window and collection efficiency through the dynode foils.

When the PSD was installed in the electron beam, several high statistics runs were taken with a very loose trigger, allowing the beam to spread across the entire active area. The overall response of the PSD includes variations in tile performance and optical contacts, as well as the MCPMT gain variations. The ratio of maps made during the test beam run to the gain maps produced in the lab therefore represent the gain uniformity of the PSD tiles and their assembly technique. In Fig. 5 this ratio is presented for the four sectors of the Philips tube (sectors A and B read out the 20 y-tiles, and sectors C and D read out the 32 x-tiles). This plot shows that the y-tiles were consistently lower by 26% than the x-tiles in the second PSD prototype, whereas in the

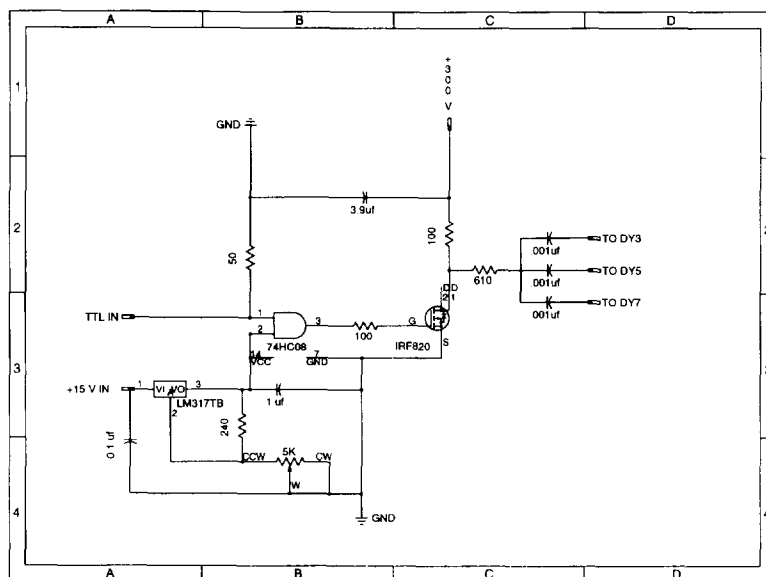


Fig. 7. Voltage pulser design.

first prototype both planes were equivalent and matched the higher x -plane light response. The average variation in tile performance (σ_{N-1}/μ) is approximately 8% for both x and y -planes.

6. A gating circuit for the MCPMT

During the first phase of the g -2 experiment, pions will be injected into the ring, initiating a massive burst of charged particles. The phototubes must be gated off for approximately 5–10 μ s to prevent damage and to maintain a consistent baseline while powered. MCPMT gating is accomplished by applying a large AC-coupled negative voltage pulse (150–300 V) into the voltage divider at dynodes 3, 5, and 7 (see Fig. 6). Diodes and extra reservoir capacitance are added in order to minimize the effects of the voltage pulse on the rest of the divider chain. The pulse causes a reverse bias between adjacent dynodes (3–4, 5–6, 7–8) which serves as a barrier to the electrons. As the gating voltage is increased, the gain is reduced, with a dramatic reduction occurring near the inter-dynode voltages (every 130 V at normal operating voltage). Gating has been optimized at roughly two dynode drops, where the gain is reduced by 5.5×10^5 . It should be noted that the gating voltage reported in Section 6.1 refers to the supply voltage as opposed to the voltage seen at the dynodes. Supply voltages of 300, 250, and 200 correspond to dynode voltages of 260, 220, and 200 respectively.

Voltage pulses are produced by driving a n -type power MOSFET with a TTL driven CMOS AND gate operating at 6.5 V (see Fig. 7). Both rise and fall times are 600 ns, and the off state can be maintained for roughly 40 μ s without disrupting subsequent gain. The stability of the off state is

ultimately determined by the supply current and how quickly the dynode charge is eliminated. Gating induces a transient on the output signal at the leading and trailing edge of the gating pulse.

6.1. Tube response to an intense, short-duration radiation burst

There are several problems associated with gating off a phototube in the presence of an intense burst of particles and radiation. Residual space charge effects due to incomplete gating can partially deaden the tube response to signals arriving soon after the gating is removed. The same effective gain reduction can also be produced by sagging in the potential between the photocathode and the first dynode. Sagging is mainly a problem in alkali photocathodes where the resistivity is high, such that the negative charge on the photocathode takes some characteristic RC time to be replenished by the external circuit. It should not be a problem for multialkali photocathodes like S20.

In addition, residual space charge produced early in the chain can appear at the anode once gating is removed, producing a slowly decaying background upon which the signals ride. A similar background could also be produced by long-lived physical processes occurring in the material close to detector. For example, Compton scatters in the detector, caused by nuclear interactions inside the calorimeter, can occur microseconds after the initial pulse. This produces light which can contribute to a long-lived background seen when the gating is removed.

A sample trace of the gated MCPMT response to the presence of a particle burst produced by a single bunch, fast-extracted beam at Brookhaven is shown in Fig. 8. The summed anode output of the MCPMT was sensitive to all

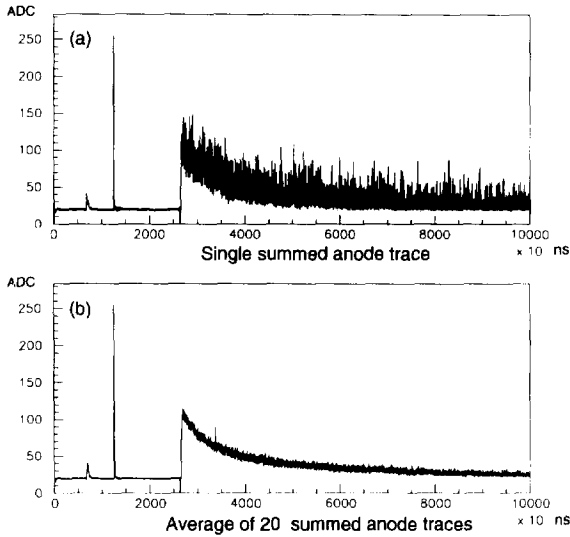


Fig. 8. Signal trace of gated MCPMT summed anode output (inverted) when PSD is subjected to 3.5×10^6 charged particles in a 70 ns burst: (a) one event (b) the average of 20 events.

the tiles from a full PSD, plus an additional tile with an attached light emitting diode (LED). Moving from left to right along the trace, we see a small peak generated by the leading edge of the MCPMT gating circuit voltage pulse. The second peak is called the “leak through”; it corresponds to the residual charge from the initial flash of light, which passes through the dynode chain while the gating circuit is still on. The integrated charge under this peak, Q_{LT} , is linearly related to the number of minimum ionizing particles (MIPs) in the burst:

$$\text{MIPs in burst} = Q_{LT}(\text{pC}) \times (\text{MIPs/pC}) \\ \times (\text{ungated gain/gated gain}),$$

where the number of pC per MIP was determined in the lab using the Ruthenium “beamline” mentioned above. That Q_{LT} is a good variable was confirmed by observing its linearity with respect to an ion chamber installed in the test beam. In addition, the absolute calibration of the ion chamber in MIPs was consistent with that calculated using Q_{LT} . After the leak-through pulse, there is a second (negative-going) transient from the trailing edge of the MCPMT gate pulse which is immediately followed by a positive background tail. The components of this tail are a combination of residual charge in the tube and light from exterior physical processes. When averaging multiple events, the LED pulse is visible on top of the quasi-DC level of the tail (Fig. 8b).

The object of the following lab tests was to create a “lab flash” calibrated to the flash at the test beam and use the subsequent MCPMT response to optimize the gating at various flash intensities as a function of gain, anode voltage, and gating voltage. The lab flash was created by shooting a 337 nm laser into a 3 cm block of BC404 scintillator. The

resulting light was guided via three 2 mm fibers to a stand in front of the MCPMT, where its intensity could be adjusted by a set of neutral density filters. Three different lengths of fiber were bundled together such that the laser pulse (~ 10 ns FWHM) could be broadened to more resemble that delivered by the Brookhaven fast-extracted beam. Q_{LT} was used to determine the amount of charge required to simulate the Brookhaven burst, which corresponded (at full intensity) to 3.5×10^6 particles passing through two $22.5 \text{ cm} \times 13 \text{ cm}$ planes of 8 mm thick plastic in approximately 70 ns, producing 2.7×10^9 photons impinging on the face of the tube. For such a pulse, Q_{LT} was ~ 500 pC at the anode after gating. The gating corresponded to a gain reduction factor of 5.5×10^5 .

6.2. Tube recovery

In order to measure the degree of flash-induced signal suppression, we plotted the detected signal from an LED which was pulsed shortly after gating was removed, in a variety of MCPMT operating conditions. The MCPMT was gated off $5 \mu\text{s}$ before the laser flash and gated back on $9 \mu\text{s}$ after the flash. A LED was then pulsed at a time after the flash ranging from $10\text{--}50 \mu\text{s}$. The ratio of LED pulse height in the presence of the flash to LED pulse height without the flash (measured by averaging ~ 300 samples on an HP54540A oscilloscope) was plotted as a function of time after flash. An unaffected LED signal thus has the value of unity and the fractional suppression of the signal after the flash is evident. For all studies, data from an individual pixel and the summed anode are both displayed. Error bars are not included on figures, but were generally 3.5% and 1% for the individual pixels and summed anode respectively. It is apparent in all the plots that the individual pixels are less adversely affected by residual charge than the summed anode.

The most obvious parameter to vary in this study is the voltage of the gating pulse itself. Fig. 9 shows the LED response to the lab flash at a fixed gain and anode voltage for several gating voltages. Clearly it is better to run at a higher gating voltage, thus minimizing the amount of charge moving through the tube. Therefore, the gating was maintained at 300 V for the remaining tests.

The anode can be operated at an adjustable positive voltage. With the anode at 0 V, both the segmented dynode and anode act as electron collectors and both pixel and anode signals are negative. With a positive voltage applied to the anode, the segmented dynode provides an additional stage of gain and the pixel output becomes positive. Fig. 10 shows the LED response to the flash for a range of anode voltages at overall operating voltages of 1300 and 1450 V. Since a gating pulse of 300 V is a smaller proportion of the total voltage in the 1450 V case, the LED response is worse. At first glance it would seem that we should run with an anode voltage of 0 V, since there was no measurable drop off in tube response. Unfortunately, overall pixel gain is reduced

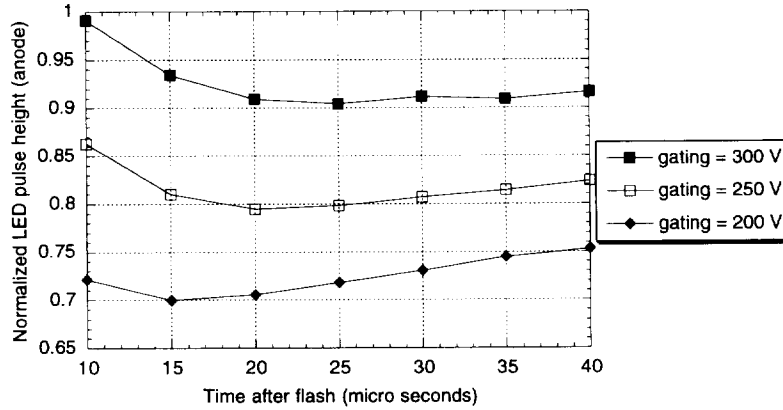


Fig. 9. Normalized LED pulse height as a function of time after flash for varying gate pulse voltages (HV = -1300 V, Anode = +30 V).

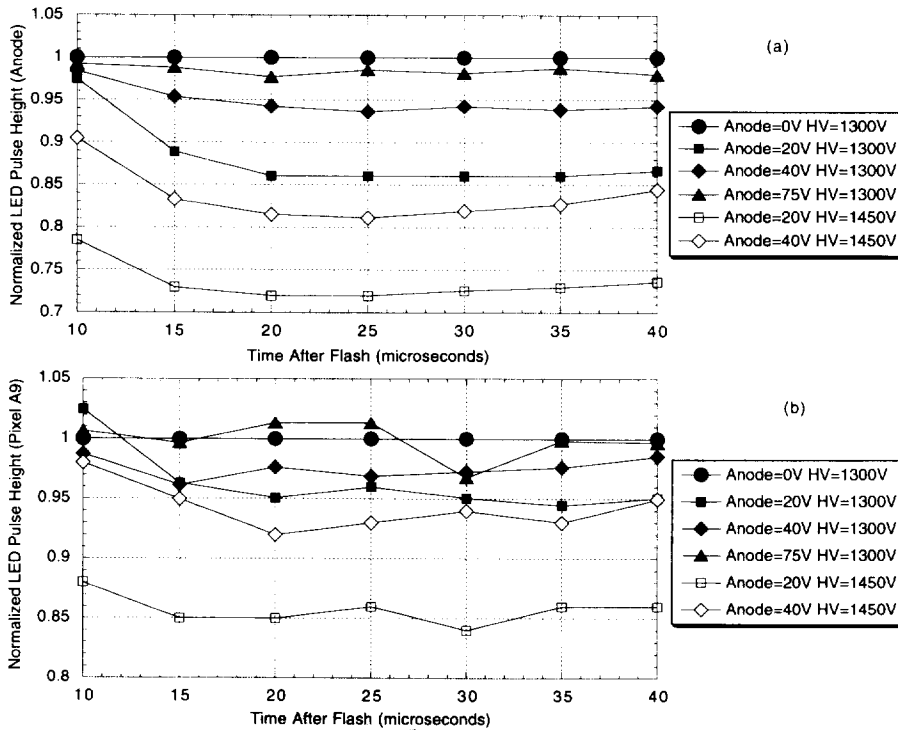


Fig. 10. Normalized LED pulse height as a function of time after flash for varying anode voltages and two different HV conditions. (Gate Pulse = 300 V).

by a factor of ~ 6 in this mode. As soon as a small amount of positive voltage is applied to the anode, the LED signal reverses sign and is affected badly by the flash. As the anode voltage is increased, the response again improves. These studies suggest that reduction in tube response is due to the elimination of charge at the end of the tube, rather than photocathode resistivity, since the response is best when either the segmented output is operated as an undiluted collector or the anode has enough potential to draw the charge through the dynode to the last stage. Fig. 10b shows that at 1300 V, it is possible to maintain the LED signal readout through individual channels at $> 95\%$ of its ungated value for all an-

ode voltages. Though not on scale, the signal recovery time constant is $\sim 200 \mu\text{s}$.

Fig. 11 shows the response to the flash at two flash intensities and at optimized voltage settings. This shows what our operating range should be for 2.7×10^9 and for 3.2×10^{10} photons striking the photocathode. Therefore, even for an order of magnitude more flash than we expect in the actual experiment, individual and anode signals should be reduced by no more than 5% and 30% respectively. With a typical pixel signal of 120 mV and a discriminator threshold of 20 mV, we should be unaffected by signal suppression.

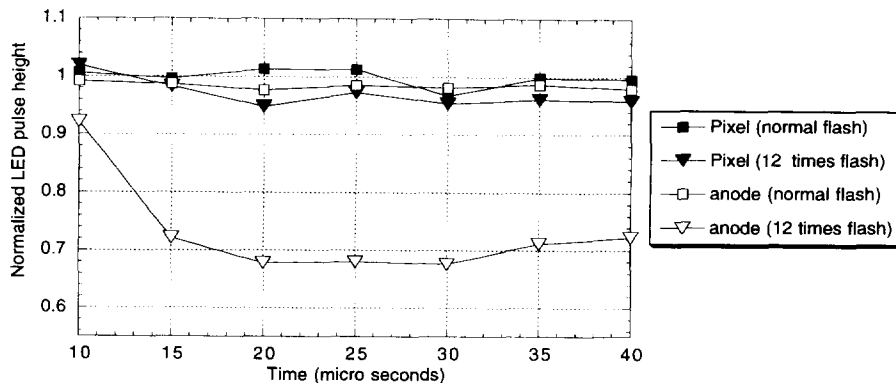


Fig. 11. Normalized LED pulse height as a function of time after flash for the expected flash and for 12 times the expected flash. Optimized operating conditions of HV = -1300 V, Anode = +75 V, Gate Pulse = 300 V.

6.3. Photocathode resistivity of the MCPMT

In order to determine whether photocathode resistivity was partially responsible for the signal suppression, the total charge at the anode was maintained at a constant value, comparable to that observed in the fast-extracted beam while gating was occurring. The temporal behavior of the MCPMT was compared to a standard bialkali tube (Hamamatsu R1355) for two different conditions: high light intensity and low gain vs average light intensity and normal gain.

An LED pulse of 100 μ s was applied to an ungated R1355 through a calibrated neutral density filter (1/110). The LED signal amplitude was adjusted such that the total integrated charge at the anode was equal to the leak-through charge (Q_{LT}) seen by the same tube operated WITH gating during the fast-extracted beam. Since the R1355 was used to read out one complete plane of the PSD during one of the Brookhaven fast-extracted tests, it could be easily normalized). The solid line in Fig. 12a shows the time response. Next the neutral density filter was removed and the gain of the tube reduced to put the two plots on the same scale. The dashed line in Fig. 12a, corresponding to two orders of magnitude more light intensity, shows that an effective gain suppression develops over the duration of the LED pulse. Since the total charge at the anode is the same in both cases, the effect is occurring at or before the first stage in the dynode chain. The same procedure was repeated for the Philips MCPMT at 1450 V and no sagging was seen in the summed anode response in Fig. 12b. The scales are different in the two cases because the Philips tube had to be run in the negative mode (no anode voltage = lower gain) in order to properly read out the anode itself. However, the total amount of light falling on the photocathode is the same in both cases. High resistivity therefore does not seem to be an element contributing to the signal suppression for the MCPMT, even though it can be a problem for other bialkali tubes with different internal structure.

7. Test beam results

We tested a full calorimeter station, including a lead scintillating fiber calorimeter and PSD, at Brookhaven National Lab (BNL). Electrons and pions (in a ratio of 1:1.7) with energies between 1–5 GeV were delivered to the B2 beam line by the AGS accelerator. The “beam trigger” consisted of a simple coincidence between two large scintillation counters located just in front of the detector. Additional narrow scintillator “fingers” (about 1 cm wide) were used whenever a smaller beam spot was needed. Fine position information (2 mm in one dimension) was obtained by using a scintillating fiber mounted directly on the upstream face of the detector and read out by a photomultiplier tube. A second hodoscope, consisting of five 28 cm wide scintillator paddles, was positioned between the PSD and the calorime-

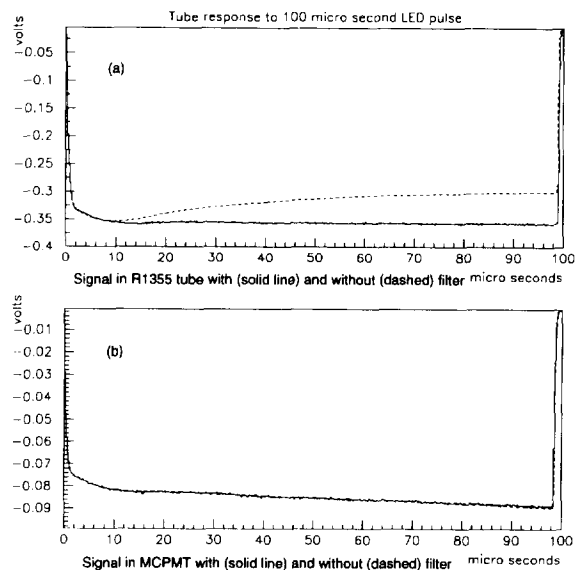


Fig. 12. Bialkali photocathode response to a 100 μ s LED pulse for two different light intensities and compensated gains. (a) is the R1355 and (b) is the Philips 1723/D1.

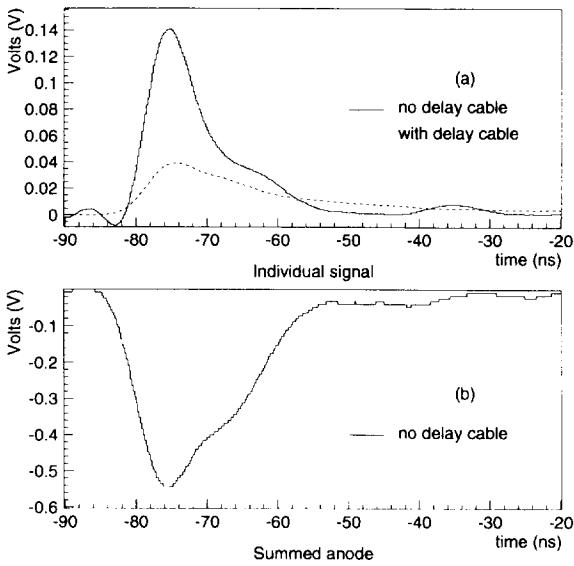


Fig. 13. Scope shots of an electron passing through a PSD tile as seen by (a) an individual MCPMT channel with and without a 230 ns delay cable and (b) the summed anode (corresponds to an electron passing through 2 planes).

ter. Called the FSD (Front Slab Detector), its purpose is to improve the timing resolution of $g-2$ decay electron events, as well as provide additional double pulse rejection. As an additional element in the test beam, it also provided a means of eliminating particles which did not make it through the PSD. A threshold Cherenkov counter improved the ratio of electrons to pions to 2.4:1. A veto counter, consisting of a 9 mm hole in a 21 cm \times 20 cm paddle read out at both ends, reduced beam halo and multiple hits. All trigger elements were also read out by ADCs and could therefore be used to make offline software cuts, if not included as online triggers.

In order to thoroughly understand the response of the PSD to minimum ionizing particles, the pulse height from all the channels was analyzed. Four 50 Ω coaxial ribbon cables⁷ delivered the 32 x -plane signals to a positive mode charge integrating ADC⁸ and the 20 y -plane signals were inverted and read out by a negative mode ADC⁹. The negative-going summed anode signal, transmitted via the same ribbon cable, was also read out by the negative mode ADC. Since the trigger requirement included the downstream Cherenkov detector and a variety of coincidence circuits, it was necessary to delay our signals by 190 (y -plane) or 230 (x -plane) ns. The attenuation was considerable, reducing a 150 mV, 13 ns FWHM signal to a 40 mV, 28 ns FWHM (Fig. 13a).

This delay and the ADC readout is specific to the particular test beam configuration herein described and will not

be used during the actual $g-2$ experiment, where the PSD will operate as an inherently digital device. Instead, a set of four NIM modules (16 channels each) will be located close to the MCPMT to discriminate and buffer the signal. A 64-bit hit pattern word per event will then be transferred via ATT twisted pair cable to a VME memory module, and read out in the data stream with the calorimeter information. We therefore expect to be able to run at a lower MCPMT voltage and still maintain the good separation between pedestal and signal which we obtained during the test beam when we were forced to use delay cables. Timing information can be obtained from either the individual strips with risetimes of 3.8 ns or from the summed anode signal with a risetime of 6.0 ns (Fig. 13b).

The beam profile for the beam trigger alone was almost 10 cm wide. It was measured by the PSD by simply incrementing in the histogram any PSD channel which had an ADC value above threshold. It is shown in Fig. 14. For the detailed PSD studies described below, a much cleaner trigger was required. By positioning the 2 mm diameter trigger fiber parallel and directly in front of a PSD tile, we were able to insure that triggered events passed through only one tile, allowing efficiency measurements on a tile by tile basis. The position of the trigger fiber and one of the 1 cm finger counters can be immediately seen by observing the beam profile in the PSD when these counters (perpendicular to each other) are included in the trigger in coincidence with the simple beam trigger (Fig. 15).

Attenuation measurements can be done on the perpendicular plane in conjunction with the efficiency measurements, since the fiber represents a 2 mm slice through 4 adjacent perpendicular tiles. The PSD array was mounted on a remotely controlled x - y translation table. With the trigger fiber aligned horizontally, moving the table in the y direction represents an attenuation scan of 4 vertical tiles (x -plane), while each individual run within the scan represents an efficiency measurement of the horizontal tile (y -plane) aligned with the trigger fiber. In addition, by comparing the response of the selected tile to its nearest neighbors on the tube face or the adjacent tile on the PSD assembly, we could study various sources of crosstalk.

7.1. Attenuation studies

Attenuation data on individual tiles was collected in the manner described above. Additional software cuts requiring a hit above threshold in the FSD hodoscope and no additional hits in other PSD tiles reduced the size of the pedestal and eliminated the crosstalk shoulder, but did not change the mean of the signal distribution. In Fig. 16, a representative sample (all curves were very similar) of tile attenuation curves are plotted on a semi-log scale. The distance along the tile is given in cm away from the light guide end of the tile, as measured by the weighted average of the three central tiles in the beam profile along the other (perpendicular) plane. The values along the vertical axis correspond to the

⁷ Cable type 1-226298-7 from AMP Inc., P.O. Box 3608, Harrisburg, PA 17105, USA.

⁸ CAEN 205A ADC. Costruzioni Apparecchiature Elettroniche Nucleari S.p.A., Via Vetràia, 11, I-55049 Viareggio, Italy.

⁹ LRS 2249W, LeCroy Corp., 700 Chestnut Ridge Rd., Chestnut Ridge, NY 10977-6449, USA.

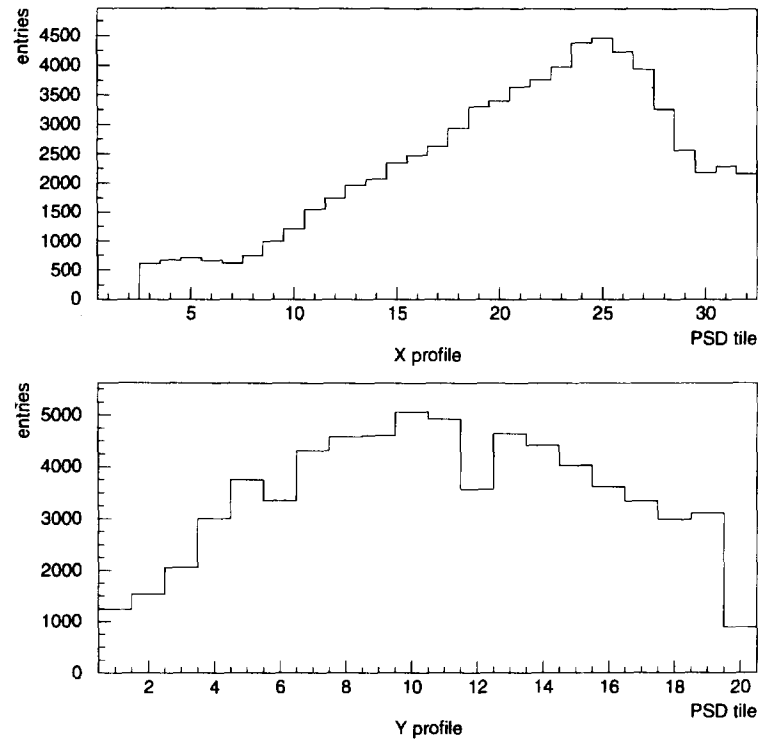


Fig. 14. Beam profile for “beam” trigger events as measured by the PSD (in units of 7 mm tiles).

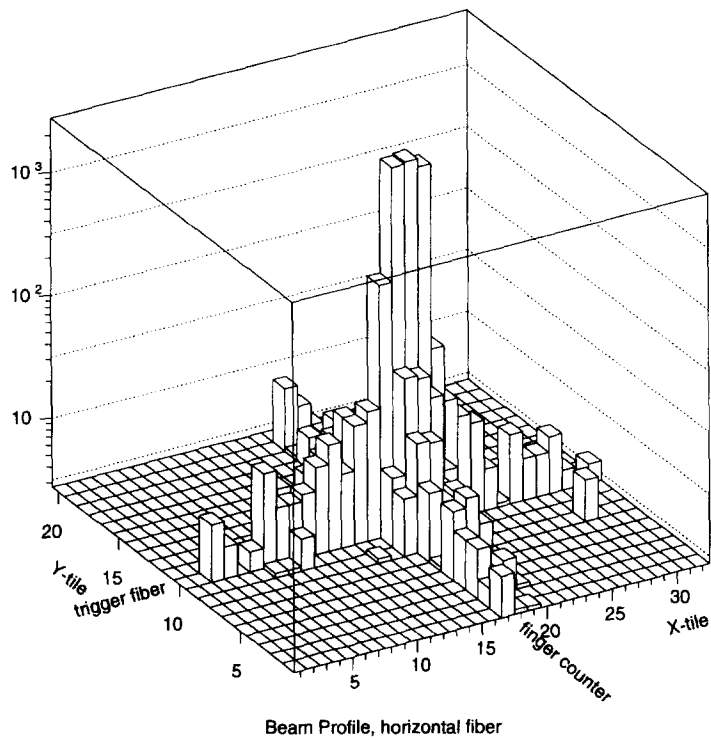


Fig. 15. Beam profile measured by the PSD in units of 7 mm tiles on a semilog plot. The 2 mm trigger fiber and 1 cm finger counter are in coincidence with the “beam” trigger.

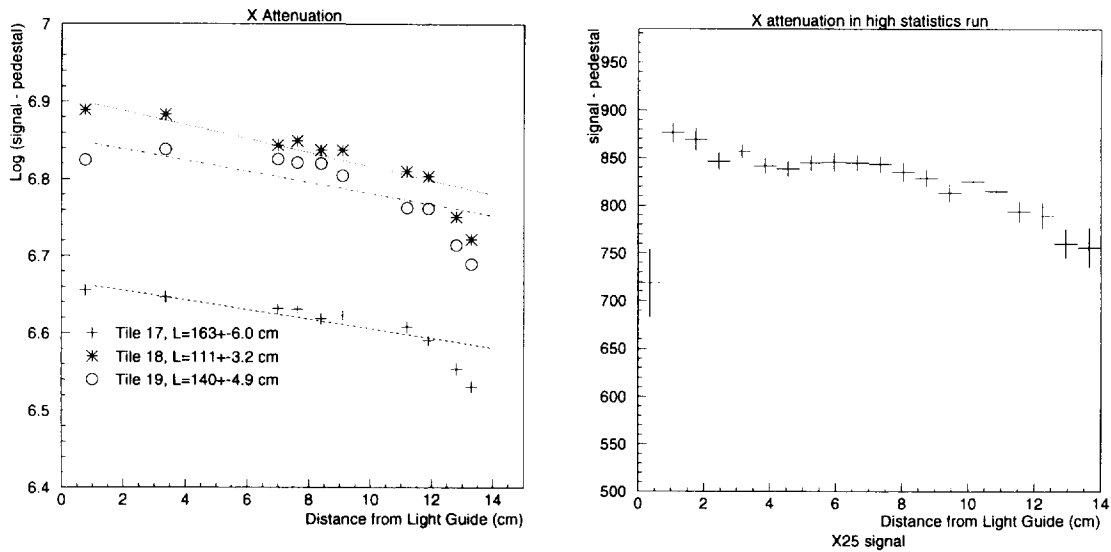


Fig. 16. Sample attenuation curves for PSD x-tiles.

mean of a Gaussian fitted to the ADC signal for that run. The errors are $< 1\%$ and too small to display in this graph. Although we recognize that the actual mathematical form for fiber attenuation is more complicated, a simple fit to an exponential decay curve ($y = Ae^{-x/x_0}$) allows us to extract an effective attenuation length x_0 . The quoted uncertainty in the attenuation length is calculated from the error on the slope given by the output of the fit.

Several features can be pointed out. First, there is an edge effect at the end of the tiles. This $\sim 10\%$ drop in signal is present in both x-tiles (13 cm long) and y-tiles (23 cm long) when the beam passes less than 1.5 cm from the aluminized end. None of these edge points were included in the exponential fit. Secondly, if one discounts the edge effect, the overall attenuation is extremely small, only 6% by the end of the longest fiber. The fitted attenuation lengths of all tiles correspond to 1–2 m. The values are extremely stable upon repeating the measurement and the fluctuations seen along the curve appear to be associated with specific defects (bubbles or scratches) in the particular tile.

As a check on the tile by tile attenuation studies, a high statistics run, where the beam illuminated the entire PSD active area, was also analyzed. For each event, its position along the length of the tile was given by the position of the center of the hit tile in the other (perpendicular) plane. As an example, the signal in tile X25 as function of distance from the light guide end of the tile (in units of y-tiles) is shown in Fig. 16b. Tile Y20 is closest to the light guide end of the x-plane. Again, edge effects of $\sim 10\%$ occur in the last few cm and ordinary attenuation losses never exceed $\sim 5\%$.

In the lab, we also measured the response of the tile as a function of the position of the electron across its width. The light output was uniform across the tile up to one millimeter from the edge. This is confirmed by a number of crack studies done during the test beam. When two tiles are being

illuminated equally, the summed anode inefficiency corresponds to the gap between the two; there is no evidence that the ADC distributions of the two tiles have low end tails corresponding to sharing the charge or that they shift below threshold due to a reduced light level near the edge.

7.2. Efficiency

The efficiency was determined both on a tile by tile basis by using the trigger fiber described above and on a plane by plane basis using the high statistics run where the beam illuminated the entire active area. In order to calculate the efficiency of a single tile, multiple tracks were removed from

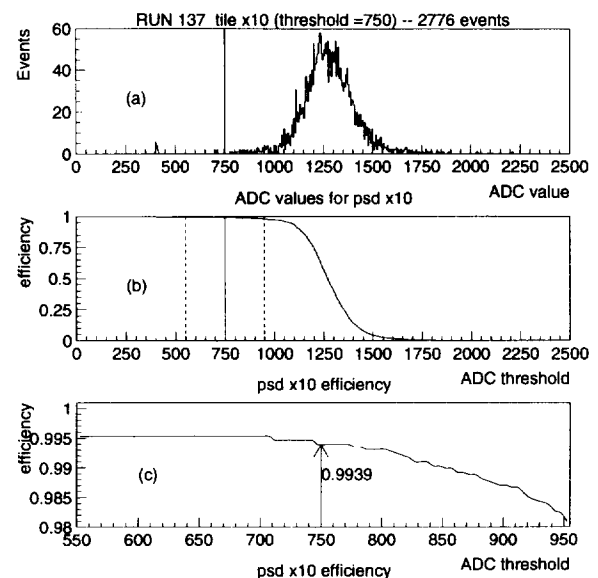


Fig. 17. ADC spectrum and efficiency for an individual tile.

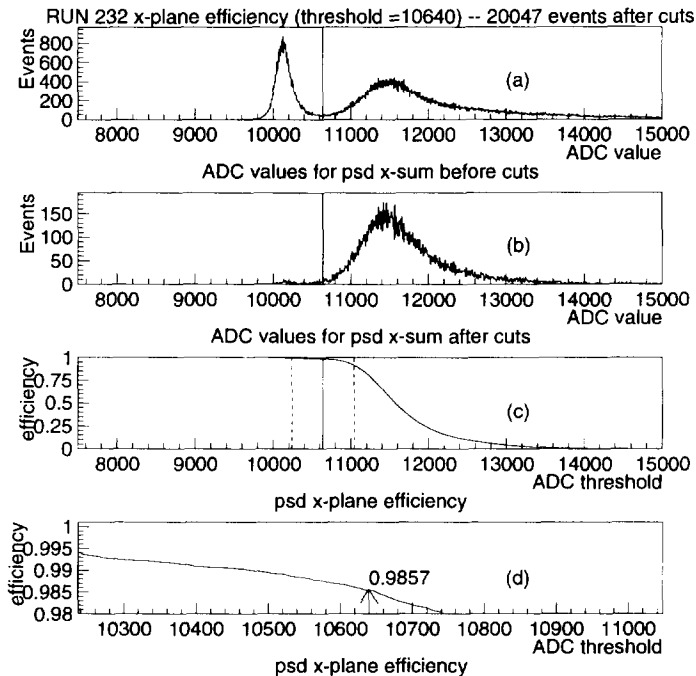


Fig. 18. Average ADC spectrum and efficiency for the PSD x-plane.

the sample by requiring one hit in the FSD and in the other plane of the PSD, but no additional hits in the same PSD plane. In addition, a cut on the pulse height in the calorimeter selected only electrons. After cuts, the remaining events below threshold in Fig. 17a are a measure of the inefficiency of the tile. In Figs. 17b and 17c the efficiency as a function of threshold cut is shown. The choice of threshold also depends on the efficiency of rejecting false hits. This is a

function of crosstalk and albedo, and details can be found in Section 7.4.

A major source of error in the above procedure is improper alignment of the trigger fiber. Some of the inefficiency could easily be particles that simply do not hit the tile if the fiber trigger is near an edge or is tilted. The ADC distribution from the high statistics run is shown in Fig. 18a, where both signal and pedestal width are broadened by channel to channel

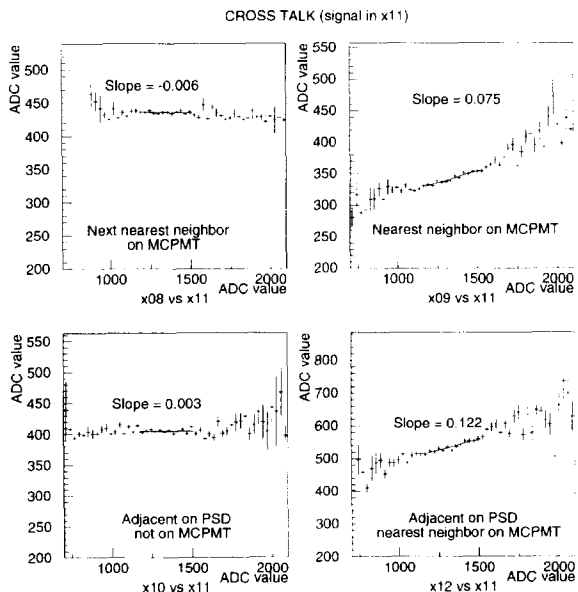


Fig. 19. Examples of crosstalk for several tile and MCPMT mapping configurations. The beam is centered on X11.

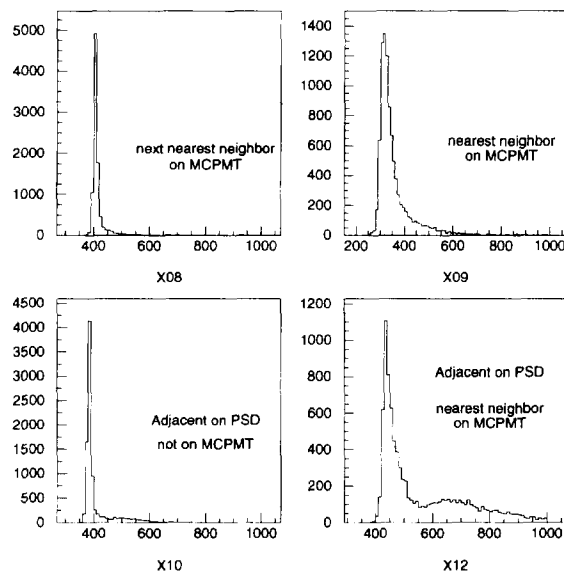


Fig. 20. Crosstalk correlation plots.

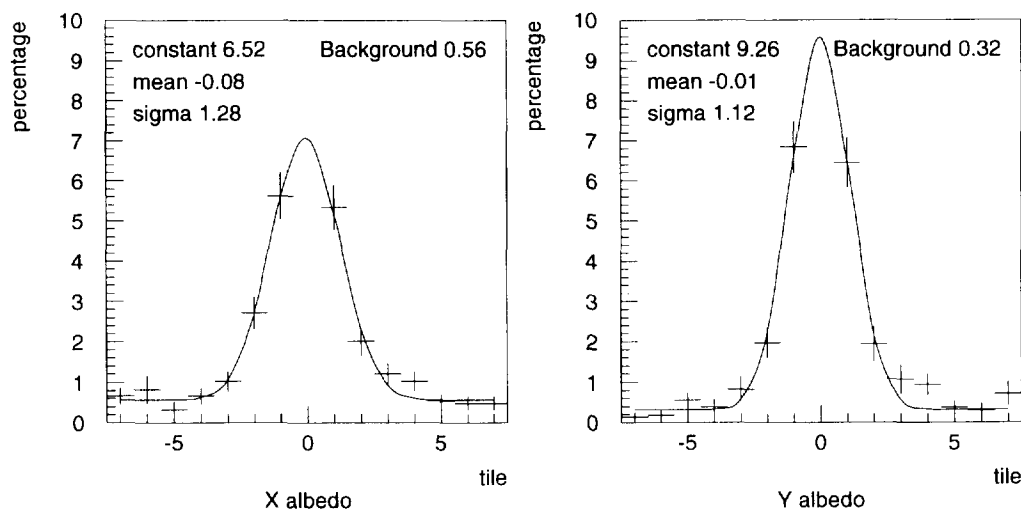


Fig. 21. Backsplash profiles in x and y from 2 GeV electrons. The fit represents a Gaussian on top of a flat background.

variations in gain. In order to determine the plane efficiency from this run, we required one hit in the opposite PSD plane, one hit in the FSD and an amount of energy deposited in the calorimeter corresponding to an electron shower. Fig. 18b shows the ADC spectrum after these cuts. In Fig. 18c and 18d the efficiency curves for the x -plane are plotted. For both x and y planes, a threshold set at 56% of the pedestal-subtracted signal gave an efficiency is 98.6%. If one assumes that the inefficiency is solely due to geometrical gaps in the hodoscope, this corresponds to a gap width of $102 \mu\text{m}$. Measurements during assembly of the PSD gave an average of $110 \mu\text{m}$ due to paint thickness and tile width tolerance, which is entirely consistent with the test beam results.

7.3. Crosstalk

There are two possible sources of crosstalk in the beam test: (1) crosstalk between neighboring PSD tiles due to insufficient optical isolation and (2) crosstalk between neighboring pixels of the MCPMT due to insufficient isolation of the secondary emission channels inside the tube. As stated in Section 4, the electrical crosstalk was measured to be $< 1\%$. Fig. 19 shows ADC plots for four channels close to the hit tile, X11. Nearest neighbors on the tube face, X09 and X12, show clear broadening of the pedestal due to crosstalk, compared to X08 and X10 which correspond to a next nearest neighbor and a well-separated channel respectively. X10 and X12, which represent PSD strips on either side of X11, exhibit a secondary bump in the pedestal (the signal is near channel 1300). The ADC correlation between these channels and the signal in the hit tile is shown in Fig. 20, where the slope corresponds to the degree of crosstalk. There is a positive correlation only for channels which correspond to nearest neighbors on the tube face. Crosstalk levels are between 5 and 15%, and about 10% on average. The secondary

bump on adjacent PSD tiles is therefore not optical crosstalk, but albedo from the developing electron shower and multiple particles in the test beam (upstream showering).

7.4. Albedo

Since the purpose of the PSD is to reject multiple hit events, it is important that it not be sensitive to scattered events and delta rays from the developing electron shower in the calorimeter or FSD. The downstream surface of the PSD is located 3.3 cm away from the FSD and 4.9 cm from the upstream face of the calorimeter. Thin plastic walls 3 mm thick isolate the PSD module from the calorimeter station.

Using a set of 4 wire chamber planes with 1 mm wire spacing in combination with the halo veto counter described above, we were able to reduce the number of multiple particle events. We required an electron identification in the Cherenkov counters, a single hit inside the beam spot in all of the wire planes, and that the number of hits in the x and y planes of the PSD be the same or differ by only one hit. We attributed the remainder of multiple hits in the PSD to albedo and noise in the setup. The profile of this backsplash, where the extra hits in the seven tiles to the left and right of the triggered tile are normalized to the number of events in the center tile, is shown in Fig. 21. Since the trigger fiber was not used in these runs, we need to account for albedo in the central tile and uncertainty about the impact point in adjacent hit tiles. We therefore assume that the probability for having a hit in one of the side tiles with backsplash into the center tile is roughly equal to the probability of having the backsplash in the side tile and the hit in the center tile. The correction is applied iteratively to determine what percentage of the side hits are actually albedo events. The effect of this correction is usually very small ($< 0.1\%$), however in neighboring tiles with a somewhat wider beam the effect

can be of the order of $\sim 2\%$. Noise appears as a flat background with the albedo from the calorimeter peaked about the impact point of the electron. The data is fit to a Gaussian with a flat background. The total number of electron triggers having two or more hits can be calculated to be $13.7 \pm 1.0\%$ in the x -plane and $15.8 \pm 1.0\%$ in the y -plane. These numbers include both noise and backplash. Looking at the fits, one can estimate that there is only a 0.5% chance of seeing a false hit far from the electron impact point, but the albedo raises it to 5–6% in adjacent tiles.

8. Conclusions

We have designed and built a tile-fiber hodoscope to meet the stringent requirements posed by the g-2 experiment. The high light yield achieved for minimum ionizing particles (30 pe per plane) provides a signal which is clearly separated from pedestal, allowing us to use a multichannel phototube from the Philips XP1700 series for readout, despite the 5–10% crosstalk present in pulsed mode. The overall plane efficiency for hit identification was 98.6%, consistent with 100% efficiency inside the tiles and 0% efficiency in the 110 μm cracks. The data format for the g-2 experiment will be purely digital: one bit per channel which states whether or not the PSD strip was above threshold. Since the OR of the ADC signals from all the tiles in a plane (see Fig. 18) were

not corrected for the gain variations in the tube prior to the above quoted efficiency calculation, this represents the efficiency we expect using a single hardware threshold for all pixels. Thus, the non-uniformity of gain within the MCPMT proved not to be a problem, partly because a majority of the pixels are within 50% of each other and we can eliminate the few bad channels by proper mapping of our 52 channels to the tube's 64 channel array. Crosstalk between PSD tiles and MCPMT channels and attenuation along the tile were also examined, and found not to affect the overall efficiency. However, albedo can decrease the rejection efficiency from $> 99.9\%$ to 94% for adjacent PSD tiles.

We have built and tested a gating circuit for the Philips XP1700 multichannel phototubes, capable of reducing the tube gain by a factor of 5.5×10^5 with a switching time of only 600 ns. Tube recovery has been characterized and gating optimized for intense bursts of light of up to 3×10^{10} photons delivered in 70 ns.

References

- [1] E821 collaboration, Design Report BNL AGS E821 (March 1995).
- [2] G. Comby and R. Meunier, Nucl. Instr. and Meth. A 269 (1988) 246.
- [3] P. Cushman and S. Hou, Nucl. Instr. and Meth. A 339 (1994) 456.
- [4] S. Majewski, B. Kross, R. Wojcik, A. Weisenberger and C. Zorn, Nucl. Instr. and Meth. A 323 (1992) 489.